Nonlinear Dynamic Analysis of Shale Gas Engine Combustion Stability

Shuai Liu (lstcls@ujs.edu.cn)
Jiangsu University https://orcid.org/0000-0002-4624-6458
Libin Zhang
Jiangsu University
Zhong Wang
Jiangsu University
Lun Hua
Tsinghua University Suzhou Automotive Research Institute
Qiushi Zhang
Tsinghua University Suzhou Automotive Research Institute

Original Research

Keywords: Shale gas engine, Nonlinear dynamic characteristics, Phase space structure, Poincaré map, Return map

Posted Date: February 2nd, 2021

DOI: https://doi.org/10.21203/rs.3.rs-166670/v1

Nonlinear dynamic analysis of shale gas engine combustion stability

Shuai Liu [a,b]*, Libin Zhang [a], Zhong Wang [a], Lun Hua[b], Qiushi Zhang[b]

[a] School of Automobile and Traffic Engineering, Jiangsu University, Zhenjiang 212013, China

[b] Tsinghua University Suzhou Automotive Research Institute, Suzhou 215200, China

Abstract: The traditional analysis method of engine combustion cycle variation is a statistical method based on a small amount of data. In essence, the obtained cycle variation is random data. In order to reveal the dynamic nature of the cyclical changes during the combustion of a shale gas engine, a nonlinear dynamics method was used to study the stability of the combustion process. The motion law of the phase space trajectory is analyzed, the influence of the shale gas composition on the trajectory distribution is analyzed, the return mapping point of the average indicated pressure in the cylinder is discussed. The relationship between adjacent combustion characteristic parameters is studied; the chaotic characteristics of the shale gas engine combustion process are discussed. The results show that during the working process of the shale gas engine, the in-cylinder pressure shows a similar quasi-periodic state in the entire phase space, and the working process has a certain chaotic law; with the increase of the CH_4, N_2 and CO_2 content in the shale gas, the combustion cycle variation increases, and the randomness of the engine working process increases. The phase space trajectory shows a monotonously increasing distribution of Poincaré mapping points on the $\sum XY_+$ section. With the increase of the combustion cycle, the linear relationship of the scattered points gradually increases, and the randomness of the combustion process increases. The return map points of the engine

* Corresponding author. e-mail: lstcls@ujs.edu.cn

combustion characteristic parameters are distributed in a cluster. When the CH_4 content increases, the distribution range of the average indicated pressure return map points increases. With the increase of N_2 and CO_2 content, abnormal combustion phenomena such as partial combustion or misfire occur during the engine combustion process, the uncertainty of the combustion process increases, and the combustion stability decreases. With the increase of engine speed, the correlation dimension and the maximum Lyapunov exponent increase, the randomness of the combustion process increases, and the chaotic characteristics of the engine working process are obvious; the time series of the cylinder pressure is more sensitive to the content of inert gas. With the increase of N_2 and CO_2 content in the gas, the correlation dimension and the maximum Lyapunov exponent increase significantly, the complexity of the phase space trajectory increases, and the chaotic characteristics become more obvious.

Keywords: Shale gas engine, Nonlinear dynamic characteristics, Phase space structure, Poincaré map, Return map

1. Introduction

The combustion speed of natural gas is slower than that of gasoline, which results in lower thermal efficiency of the engine, larger combustion cycle changes, and poorer stability of the engine's working process [1-4]. The composition of shale gas is similar to natural gas, the main component is CH_4, the molecule contains only one C atom, and the H/C ratio is relatively high. When applied to engines, it can improve the effective thermal efficiency of the engine and is a potential engine alternative fuel [5-7]. The distribution position and accumulation process of shale gas reservoirs are different, and the composition of shale gas is quite different. The content

of N_2 and CO_2 in shale gas in some areas is relatively high, leading to differences in the propagation speed and flame structure of shale gas premixed flames, resulting in different cyclical changes in the working process [8-9].

Changes in various components of gaseous fuel affect the calorific value of the fuel. The combustion speed of different gas components is different, resulting in a difference in the combustion process in the cylinder. By changing the composition of the combustible mixture, the combustion process of the engine can be improved and the stability of the working process can be improved [10-14]. Weaver and Santavicca et al. [15] analyzed the influence of N_2 content on the formation process of the fire core and the pressure in the cylinder on an optical engine. The research results show that with the increase of N_2 content, the maximum combustion pressure in the cylinder and the peak pressure rise rate decrease, and the combustion speed decreases, which leads to the increase of the combustion cycle variation coefficient of the engine. Li et al. [16] mixed coal-bed methane with different components and carried out experimental research on engine combustion and emission characteristics. The research results showed that when the N_2 content in coal-bed methane increases, the maximum combustion pressure and pressure rise rate decrease, the peak heat release rate decreases, the flame development period is prolonged, the emission of HC and CO increases, and the emission of NO_x decreases significantly. According to the research results, it can be found that the gas composition has a certain influence on the combustion cycle of the engine. Due to the different contents of N_2 and CO_2 in shale gas in different regions, it is necessary to study the influence of gas composition on the combustion cycle of shale gas engines.

The traditional analysis method of engine combustion cycle variation is a statistical method

based on a small amount of data. In essence, the cycle variation obtained is random data. With the development of nonlinear dynamics, many scholars have carried out related research work on the nonlinear dynamics of combustion cycle changes. Daw et al. [17] used a zero-dimensional simulation model to explore the dynamic characteristics between the cycle changes before and after the ignition engine. The research results show that there are chaotic characteristics between cyclic changes, which are different from typical chaotic models due to the influence of combustion noise. Green et al. [18] used a linear Gaussian stochastic model to study the dynamics of the combustion cycle of a spark-ignition engine. The research results show that the combustion process in the cylinder is inconsistent with the linear Gaussian random process, showing a certain nonlinear dynamic process. According to the research results of scholars, it can be seen that the combustion process of spark-ignited engines has the characteristics of complex nonlinear dynamics, and the method of nonlinear dynamics can be used for research.

In order to characterize the nonlinear dynamics characteristics of the engine combustion process, scholars have adopted different nonlinear dynamics research methods. Wangner et al. [19] used non-linear dynamics research methods such as back mapping, entropy analysis, and symbolic time analysis to explore the transient characteristics of the dynamic behavior of the engine cycle. The dynamic characteristics of the change are gradually determined. When the intensity of turbulence in the cylinder decreases, the combustion stability under lean burn conditions decreases, and the noise in the dynamic characteristics of the cycle changes gradually becomes obvious. The dynamic characteristics of the combustion cycle changes are affected by the injection time. Yao et al. [20] analyzed the correlation between the characteristic

parameters of the combustion cycle and reconstructed the time series of the in-cylinder pressure. The research results show that the average indicated pressure is linearly related to the maximum combustion pressure. When the engine is running at a fast combustion rate and complete combustion conditions, the maximum combustion pressure can fully characterize the combustion cycle changes. When the combustion in the cylinder deteriorates, the maximum combustion pressure cannot represent the combustion cycle changes. Yang et al. [21] studied the influence of ethanol substitution rate on the dynamic characteristics of the combustion system by using a nonlinear dynamics research method. The research results show that the introduction of ethanol has a significant impact on the inter-cycle combustion changes of the engine load and the system dynamics. Many scholars have not yet unified the opinions of whether the combustion process of ignition engines has chaotic characteristics. Letellier et al. [22] used the method of nonlinear dynamics to reconstruct the phase space of the time series of the engine cylinder pressure, and performed the Poincaré mapping and the return mapping of the phase space with an equivalent ratio of 0.8, and discussed the combustion dynamic characteristics of cyclic changes. The research results show that there are random factors in the combustion process of the engine, and the combustion process does not have chaotic characteristics. Liu et al. [23] used the method of nonlinear dynamics to analyze the dynamic nature of the cycle variation of different fuels in the engine. The research results show that the phase space trajectory of the cylinder pressure has a certain chaotic characteristic, and the structure of the initial stage of combustion is relatively tight. Poincaré map reduces the complexity of the phase space structure; the engine combustion process has chaotic characteristics. Wang et al. [24] studied the chaotic characteristics of the EFI natural gas engine

111 combustion system under different ignition advance angles. The research results show that in
112 the engine working process, the phase space attractor is in a limited range and has a complex
113 geometric structure that is twisted, crossed and folded. The correlation dimension of the
114 attractor is a fraction less than 2, and the maximum Lyapunov exponent is positive. The
115 combustion system shows obvious chaotic characteristics. Ding et al. [25] used the phase space
116 reconstruction method and the 0-1 test method to study the dynamic characteristics of the
117 premixed natural gas engine combustion process. The results show that by reconstructing the
118 phase space, the law of the combustion process can be clearly studied. The combustion process
119 of the premixed natural gas engine under different injection timing conditions is chaotic.
120 According to the research results of scholars, it can be seen that in the research methods of
121 nonlinear dynamics, phase space reconstruction, return mapping, entropy analysis, symbolic
122 time analysis and recursive mapping can study the combustion process of the engine. The
123 method of nonlinear dynamics is used to study engine cycle changes, ignoring the complex
124 physical and chemical models in the combustion process. Through the analysis of the time
125 series of in-cylinder pressure, the essential characteristics of the system in the process of in-
126 cylinder pressure change are proved, which provides a theoretical basis for the establishment
127 and improvement of the calculation model of cycle variation and the improvement of engine
128 combustion stability. At present, scholars focus on the research on the influence of engine
129 operating parameters on the dynamic characteristics of cycle changes. There is not much
130 research work carried out to explore the influence of gas composition on the dynamic
131 characteristics of combustion cycle changes using nonlinear dynamics. It is necessary to study
132 the non-linear dynamic characteristics of shale gas components on the engine combustion

process, to find out the nature of cyclic changes, and to provide a theoretical basis for improving the combustion stability of shale gas engines.

In this paper, the phase space reconstruction of the cylinder pressure is carried out by the delayed coordinate method, the motion law of the phase space trajectory is analyzed, the trajectory is projected on the XY plane, and the influence of shale gas composition on the trajectory distribution is studied; $\sum XY_+$ is selected Poincaré section, analyzed the projection of the phase space trajectory on the section; explored the return mapping point of the average indicated pressure in the cylinder, studied the relationship between adjacent combustion characteristic parameters; analyzed the correlation dimension and the largest Lyapunov exponent, etc. The chaotic characteristic quantity of the combustion process, and the change law of the chaotic characteristic of the shale gas engine combustion process is discussed.

2. NONLINEAR DYNAMICS AND CHAOS THEORY

2.1. Phase space reconstruction

The delay coordinate method in the phase space reconstruction theory is used to analyze the time series of the engine cylinder pressure [26-27]. The first derivative and the second derivative of the cylinder pressure time series have important physical meanings in the combustion process. Using differential coordinates to reconstruct the phase space of the cylinder pressure time series can better analyze the combustion dynamics. The reconstructed phase space Ω_{XYZ} is shown in equation (1).

$$\Omega_{XYZ} = \left\{ \left(X, Y, Z \right) \in R^3 \right\} \quad (1)$$

In order to facilitate the analysis of the changes in the phase space of different fuels, the

projection method is used to reduce the dimensions of the three-dimensional phase space structure, as shown in equation (3).

$$\Omega_{XY} = \left\{ \left(X, Y \right) \in R^2 \right\} \quad (2)$$

2.2. Nonlinear transformation

(1) Poincaré map

During the working process of the engine, the trajectories obtained through phase space reconstruction are densely distributed, the structure is complex, and the dynamic details are not clearly expressed. Direct observation is difficult. The Poincaré section method can effectively analyze the law of motion in the cylinder. Poincaré cross-section refers to the two-dimensional cross-section obtained by selecting a suitable plane in the three-dimensional phase space structure [28-29]. The intersection of the phase space trajectory and the plane is the Poincaré point. The reduction of the dimensionality simplifies the analysis of the trajectory to the analysis of scattered points, which is simpler and more effective. The $\sum XY_+$ Poincaré section is selected to analyze the dynamics in the cylinder, as shown in equation (3).

$$\sum_{XY+} = \left\{ \left(X, Y \right) \in R^2 \left| Z=0, Y>0 \right. \right\} \quad (3)$$

(2) Return map

Return mapping is an important method to analyze the correlation between the front and rear cycles of the engine [30]. The working process of the engine is a periodic movement, and the average indicated pressure (IMEP) of two adjacent cycles can be used as the horizontal and vertical coordinates to obtain a set of discrete return maps. This discards most of the in-cylinder pressure information, but it is convenient and intuitive to study the dynamic characteristics of

combustion cycle changes. The return map of the average indicated pressure is shown in equation (4) [31].

$$\begin{cases} X = IMEP_{(n)}; \\ Y = IMEP_{(n+1)}. \end{cases} \quad (4)$$

（3）Chaos analysis method

Chaos phenomenon refers to a special non-periodic motion that exists in a certain system, which is similar to irregular, but has a sensitive dependence on initial conditions. It is a manifestation of the inherent randomness of nonlinear dynamic systems [32-34]. According to the phase space trajectory of the cylinder pressure in the combustion process of the engine, it can be seen that the system moves around a limited range with "attraction", which is called an attractor. The phase space trajectory is attracted by the attractor of the pressure in the cylinder. The trajectory is close to the attractor, and the combustion process in the cylinder is stable on the attractor. It is shown that the attractor represents the stable state of the system and is a phase space region of the final destination of the dynamic system.

The correlation dimension and Lyapunov exponent are characteristic quantities that represent the chaotic characteristics of the system [35]. The correlation dimension characterizes the estimation of the complexity of the system, is sensitive to the behavior of the time course, and can better reflect the dynamic characteristics of the system; The Lyapunov exponent can quantitatively describe the separation speed of the chaotic motion trajectory, which is the basis for judging the sensitivity of the chaotic motion to the initial conditions, and it describes the instability of the motion trajectory.

3. Test equipment and plan

196 The test is aimed at a single-cylinder test gasoline engine. It adopts a simple structure and a
197 low-cost modified intake port injection mode. The shale gas is fully mixed with air in the intake
198 manifold and ignites. The cylinder diameter of the gasoline engine is 88mm, the calibrated
199 speed is 3600r/min, and the calibrated power is 7.5kW. The specific technical parameters of the
200 test engine are shown in **Table 1.**

201 **Table 1** Test engine parameters

Parameter name	Parameter
Cylinder diameter (mm)	88
Piston stroke (mm)	64
Displacement (mL)	389
Compression ratio	8.1
Rated speed (r/min)	3600
Rated power (kW)	7.5
Maximum torsion speed (r/min)	2000～2600
Maximum torque (N•m)	26

202 The shale gas engine was operated under the maximum torque and calibration conditions,
203 respectively, and the changes in the combustion process and the stability of the engine when
204 the gas components such as CH_4, N_2 and CO_2 in shale gas changed were discussed.

205 **Table 2** Each gas composition during the CH_4 content change test

Test plan	CH_4	C_2H_6	C_3H_8

1	85%	10%	5%
2	90%	5%	5%
3	95%	5%	0%

According to the test requirements, the content of CH_4 in shale gas is 85%, 90%, and 95%, respectively. When the CH_4 content change test is carried out, the N_2 and CO_2 content are not considered. The test plan is shown in **Table 2**.

Table 3 Each gas composition during the inert gas content change test

Test plan	CH_4	C_2H_6	C_3H_8	N_2	CO_2
1	90%	5%	5%	0%	0%
2	85%	2.5%	2.5%	10%	0%
3	75%	2.5%	2.5%	20%	0%
4	85%	2.5%	2.5%	0%	10%
5	75%	2.5%	2.5%	0%	20%

When the inert gas content change test was carried out, the content of CH_4 in shale gas was 90%, the content of N_2 and CO_2 were 0%, 10% and 20%, respectively. The test plan is shown in **Table 3**.

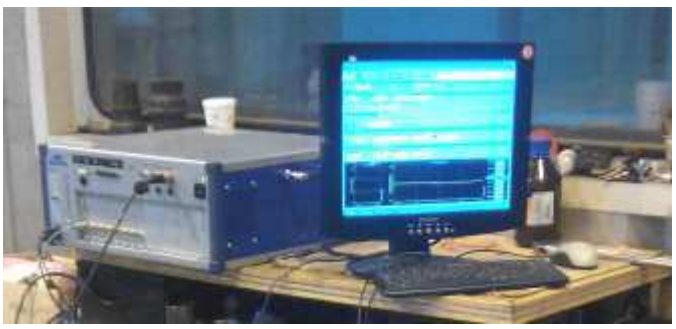

Fig. 1. DEWE800 combustion analyzer

During the test, data collection was mainly carried out on the cylinder pressure, and the cylinder pressure curve for 120 continuous working cycles was collected. Cylinder pressure data is measured by a Kistler6125B01 spark plug pressure sensor, and the cylinder pressure signal is recorded by the DEWE800 combustion analyzer. As shown in **Fig. 1**, the crankshaft angle generator interval is 1°CA.

4. Results and discussion

4.1. Phase space analysis

(1) Phase space reconstruction

Fig. 2 shows the reconstructed phase space trajectory of the in-cylinder combustion process when the engine is running at the maximum torque and the CH_4 content in shale gas changes. It can be seen from the figure that during the combustion process of a shale gas engine, each cycle corresponds to a closed curve in the phase space, and each curve has a similar development history, which is distributed in an irregular band in the phase space. The in-cylinder state of the engine reflects a quasi-periodic state, and the dynamics shows a certain chaotic law [36-37]; In-cylinder pressure is in the range of 0-2MPa, and the tip trajectory in the phase space structure is highly coincident, indicating that the engine's intake and exhaust process is stable. In the region of Y>0, the trajectory first increases in the Z-axis direction and then gradually decreases, which characterizes the mixture. In the compression stage before combustion, the arc end of the curve is larger in the X-axis direction, which represents the

combustion stage of the engine. In the region of Y<0, the trajectory gradually increases in the Z-axis direction, which is characterized by the expansion of the mixture after combustion. The phase space trajectory is relatively scattered in the arc area, indicating that combustion is the main factor that causes the engine to work instability; with the increase of CH_4 content, the trajectory of the arc end is gradually dispersed, indicating that the stability of the engine is gradually decreasing.

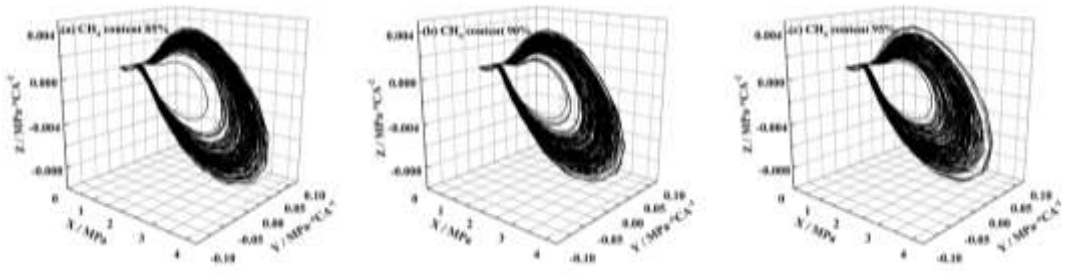

Fig. 2. The phase space of the combustion process in the cylinder under the maximum torque condition

Fig. 3 shows the reconstructed phase space trajectory of the in-cylinder combustion process when the engine is running under calibration conditions and the shale gas CH_4 content changes. It can be seen from the figure that the phase space trajectory of the combustion in the cylinder is closed and distributed periodically, showing a certain chaotic characteristic. As the CH_4 content in shale gas increases, the arc area gradually disperses; when the CH_4 content is 85% ,the reconstruction trajectory is distributed in a wide area in the phase space, the extreme values in the X-axis and Y-axis directions are large, indicating that the shale gas burns quickly in the cylinder, and the maximum explosion pressure and pressure rise rate are large; Compared with the maximum torque condition, the phase space trajectory of the combustion process is more scattered, indicating that the combustion stability of the engine decreases with the increase of speed; when the CH_4 content is 95%, the value of individual trajectories in the X-axis

direction is lower, and the Y-axis The range of value change in the Z-axis and Z-axis directions is narrow, which is a partial combustion cycle [38].

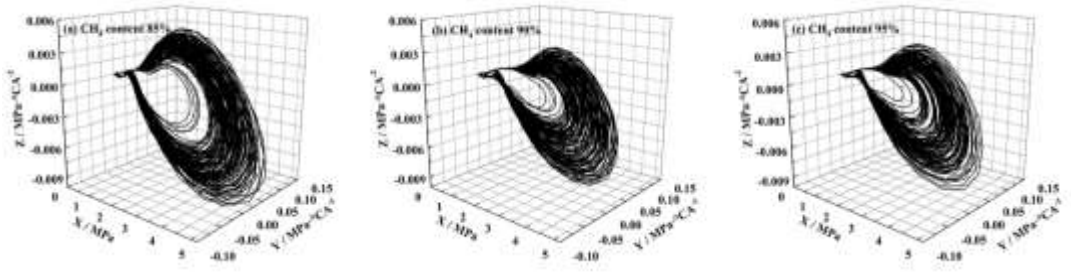

Fig. 3. The phase space of the combustion process in the cylinder under calibration conditions

Fig. 4 shows the influence of the N_2 content in the shale gas on the phase space trajectory of the combustion process in the cylinder when the engine is running under the calibrated conditions. It can be seen from the figure that when the N_2 content is 0%, the phase space trajectory distribution is relatively compact; when the N_2 content increases to 10%, the distribution range of the phase space trajectory in the X-axis direction increases, and the relatively dense area of the arc end trajectory is mainly distributed in the range of 3MPa, and the number of partial combustion cycles increases; as the N_2 content increases to 20%, the phase space trajectory is further dispersed, and the combustion stability decreases. The maximum value in the X-axis direction is significantly reduced, indicating that the increase in N_2 content, the decrease in the combustion speed of shale gas in the cylinder, the slower heat release process, the decrease in the maximum explosion pressure, and the increase in the number of partial combustion cycles. The maximum value of the arc area of individual working cycles in the X-axis direction is less than 2MPa, and the Y-axis and Z-axis directions do not increase significantly, which is a misfire cycle.

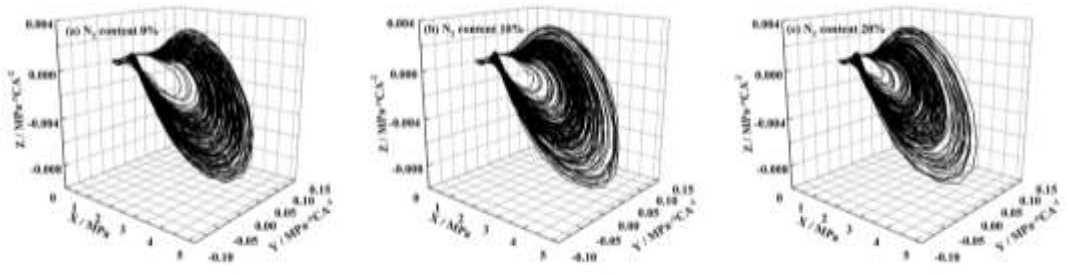

Fig. 4. The phase space of the combustion process in the cylinder when the N_2 content changes

Fig. 5 shows the influence of the CO_2 content in shale gas on the phase space trajectory of the combustion process in the cylinder when the engine is running under calibration conditions. It can be seen from the figure that with the increase of CO_2 content, the phase space trajectory gradually disperses. Compared with the influence of N_2 on the combustion phase space trajectory, under the same content condition, the phase space trajectory of CO_2 disperses and the pressure rise rate decreases. The maximum value in the Y-axis direction decreases, and the maximum explosion pressure in the cylinder decreases; during the intake and exhaust phases, with the increase of CO_2 content, the distribution of the phase space trajectory does not change much.

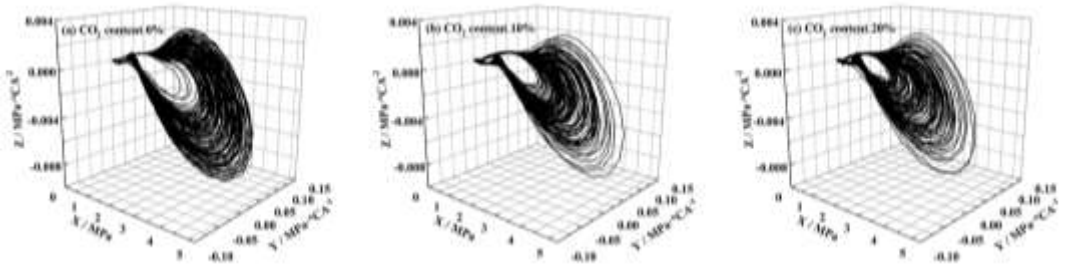

Fig. 5. The phase space of the combustion process in the cylinder when the CO_2 content changes

(2) XY plane projection

By reducing the phase space dimension of the combustion process by projecting on a plane, the change rule of the phase space trajectory is discussed. **Fig. 6** shows the projection of the

phase space trajectory of the combustion process in the cylinder on the XY plane when the engine is operating at the maximum torque and the CH_4 content in the shale gas changes. It can be seen from the figure that the projection of the phase space trajectory on the XY plane is fan-shaped. The initial stage of the trajectory has a high degree of coincidence and a relatively tight structure. When combustion occurs, the trajectory rises rapidly and gradually diverges, and is relatively scattered at the maximum value of the Y axis. Obviously, the trajectory quickly overlaps after reaching the maximum value in the X-axis direction, and returns to the starting point to form a closed curve, indicating that the combustion process in the cylinder is chaotic; when the CH_4 content is 85%, the maximum value of the trajectory in the Y-axis direction is in the range of 0.07～0.11MPa/°CA, and the distribution area in the X-axis direction is 3.2～4.0MPa; with the increase of CH_4 content, the phase space trajectory gradually diverges, which is obvious at the maximum of the X-axis and Y-axis. When the CH_4 content is 95%, in the X-axis direction, the maximum value of the trajectory is distributed in the range of 2.8～3.8MPa, and the distribution range is increased by 25%. In the Y-axis direction, the maximum value is mainly distributed in the range of 0.05～0.12MPa/°CA .

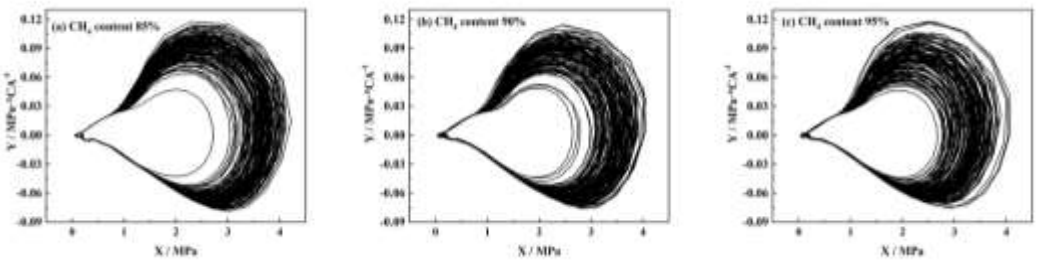

Fig. 6. Projection of phase space trajectory on XY plane for maximum torque condition

Fig. 7 shows the projection of the phase space trajectory of the combustion process in the cylinder on the XY plane when the engine is running under the calibrated conditions and the

306 CH_4 content in the shale gas changes. It can be seen from the figure that as the engine speed
307 increases, the flame propagation speed increases, the heat release rate increases, the turbulence
308 intensity in the cylinder and the residual exhaust gas volume increase, resulting in an increase
309 in the distribution range of the maximum explosion pressure and the pressure increase rate.
310 Under calibration conditions, when the CH_4 content is 85%, in the X-axis and Y-axis directions,
311 the maximum distribution is in the range of 3.5～5.0MPa and 0.06～0.14MPa/°CA; with the
312 increase of CH_4 content, the value in the X-axis direction corresponding to the trajectory
313 dispersion position increases, indicating that the flame retardation period is prolonged, and the
314 decrease of the combustion speed causes the maximum value in the X-axis and Y-axis directions
315 to decrease, the distribution range increases, and there is a partial cycle. The maximum
316 explosion pressure of is relatively small, which is a partial combustion cycle. The maximum
317 value of individual cycles in the X-axis direction is less than 2.5MPa, and the distribution range
318 of the trajectory in the Y-axis direction is small, which is a misfire cycle [39].

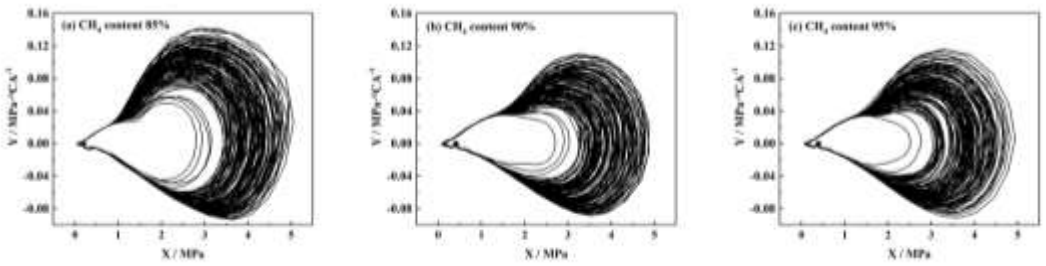

319

320 **Fig. 7.** The projection of the phase space trajectory on the XY plane of the calibration condition

321 **Fig. 8** shows the change rule of the projection of the phase space trajectory on the XY plane
322 with the N_2 content when the engine is running under the calibrated condition. It can be seen
323 from the figure that when the N_2 content is 0%, as the combustion process begins, the trajectory
324 gradually diverges, indicating that the dynamic process in the cylinder is controlled by the

combustion phase; when the N_2 content increases to 10%, the trajectory diverges significantly in the X-axis direction, and the maximum value is in the range of 2.5～5.1MPa, and the maximum value in the Y-axis direction is in the range of 0.02～0.10MPa/°CA. The N_2 in the gas suppresses the combustion process, the heat release process is prolonged, and there is a partial combustion and misfire cycle; when the N_2 content increases to 20%, the phase space trajectory further diverges, and the combustion speed decreases, resulting in a decrease in the value of the trajectory in the dense area of the X-axis and Y-axis directions, an increase in misfire cycles, and a significant decrease in engine working stability.

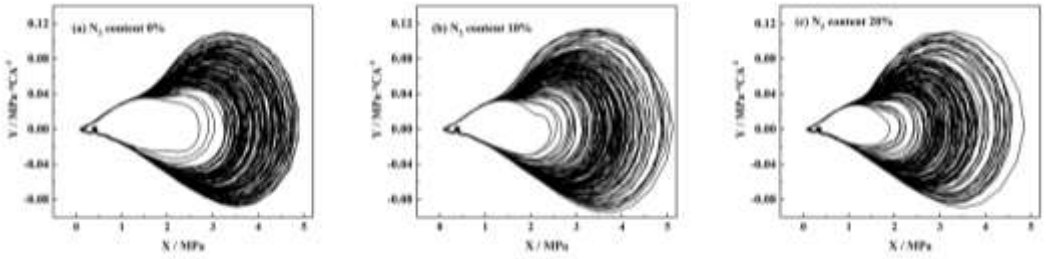

Fig. 8. Projection of phase space trajectory on XY plane when N_2 content changes

Fig. 9 shows the variation of the projection of the phase space trajectory on the XY plane with the CO_2 content when the engine is running under the calibrated conditions. It can be seen from the figure that with the increase of CO_2 content, the degree of dispersion of the trace in the later stage of combustion increases, and the distance from the obvious divergence area to the combustion start point increases. The extension of the combustion duration leads to a decrease in the stability of the engine and the reciprocating movement of the piston. The impact on the dynamics process in the cylinder increases. The combustion cycle changes are mainly affected by the flow field in the cylinder. The changes in the flow field characteristics during the formation of the fire core have the greatest impact on the cycle changes; when the CO_2

content increases to 20%, the tangent slope of the trajectory dispersion position decreases, the combustion process is difficult, the flame development period is prolonged, and the number of partial combustion and misfire cycles increases significantly; the effect of CO_2 on the phase space trajectory dispersion is significantly stronger than N_2, the combustion stability of the engine is poor.

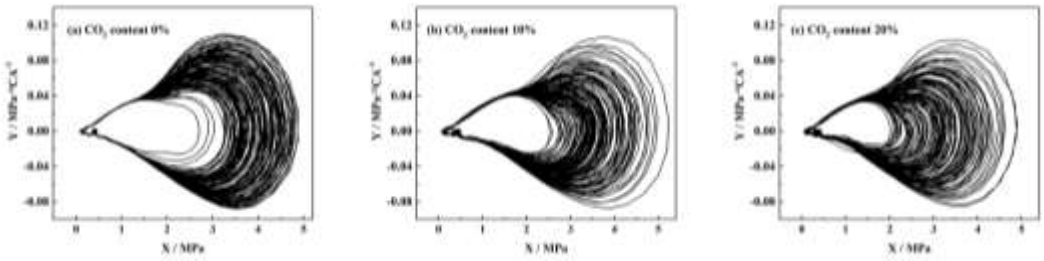

Fig. 9. Projection of phase space trajectory on XY plane when CO2 content changes

4.2. Poincaré mapping

Fig. 10 shows the Poincaré mapping of the phase space of the shale gas engine combustion process in ΣXY_+ when the engine is running at the maximum torque condition and the CH_4 content changes. It can be seen from the figure that the Poincaré mapping points are distributed in an elliptical shape in a small area, indicating that the shale gas engine is operating at the maximum torque, and the phase space of the combustion process exhibits periodic chaotic motion in the Poincaré map of the cross-section $\sum XY_+$ [40]; when the CH_4 content is 85%, the distribution range in the X-axis direction is 1.9～2.7MPa, and the distribution range in the Y-axis direction is 0.06 ～0.12MPa/°CA^{-1}, when the content of CH_4 increases, the scatter points move to the lower left corner, the maximum burst pressure and pressure rise rate decrease, the combustion speed decreases, the distribution range is gradually slender, the periodicity weakens, and the combustion stability decreases. When the CH_4 content reaches 95%, the distribution

range of scattered points in the X-axis direction is 1.75～2.75MPa, and the distribution range of the Y-axis direction is 0.04～0.12MPa/°CA^{-1}.

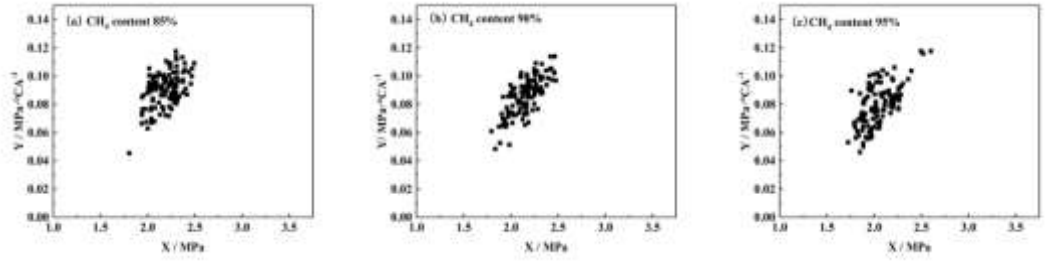

Fig. 10. Poincaré mapping of the phase space of the maximum torque condition on the section $\sum XY_+$

Fig. 11 shows the Poincaré mapping of the phase space of the shale gas engine combustion process in ΣXY_+ when the engine is running under the calibration conditions and the CH_4 content changes. It can be seen from the figure that when the CH_4 content is 85%, the distribution range of the mapping points in the X-axis direction is 2.0～3.0MPa, and the distribution range in the Y-axis direction is 0.04～0.14MPa/°CA-1, as the rotation speed increases, the distribution range of scattered points increases, the periodicity decreases, the cyclic variation of combustion increases, the stability decreases, and the values in the X-axis and Y-axis directions increase, indicating that the heat release rate increases, and the pressure in the cylinder increases; when the CH_4 content is 90%, the mapping points are linearly distributed, and the distribution law is monotonously increasing. The correlation between the pressure in the cylinder and the pressure rise rate increases. At the lower left corner of the distribution area, some scattered points rise upward; when the CH_4 content is 95%, the periodicity of the mapping point distribution is weakened, indicating that the shale gas engine is operating under the calibration conditions, and the Poincaré mapping of the combustion process phase space on the section $\sum XY_+$ shows aperiodic chaotic motion.

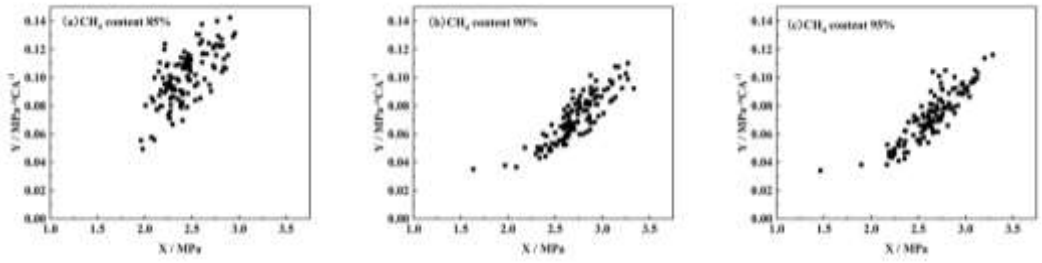

382

383 **Fig. 11.** The Poincaré mapping of the phase space of the calibrated condition on the section ∑XY+

384 **Fig. 12** shows the influence of N_2 content on the ∑XY+ Poincaré mapping when the shale
385 gas engine is running under calibration conditions. It can be seen from the figure that when
386 shale gas contains N_2, the distribution area of Poincaré mapping points is gradually slender, the
387 correlation coefficient between the pressure in the cylinder and the pressure rise rate increases,
388 and the non-periodic distribution of the scattered points increases, the upward circulation in
389 the lower left corner increases, and the distribution pattern of the scattered points gradually
390 becomes arc-shaped, and the densely distributed areas are concentrated in the ranges of 2.2～
391 3.0MPa and 0.03～0.10MPa/°CA^{-1}, in-cylinder pressure and pressure rise rate decrease; when
392 the N_2 content is 20%, the combustion speed decreases, and the arc-shaped distribution law is
393 more obvious, indicating that the non-periodical distribution of the mapping points increases,
394 the combustion uncertainty increases, and the stability of the work decreases.

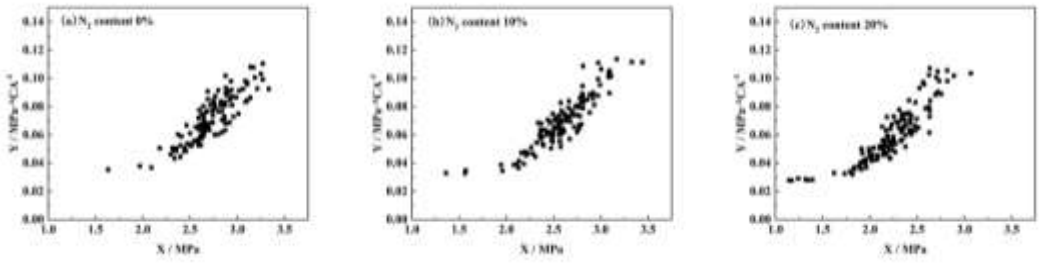

395

396 **Fig. 12.** Poincaré mapping of the phase space on the section ∑XY+ when the N_2 content changes

397 **Fig. 13** shows the influence of CO_2 content on the ∑XY+ Poincaré mapping when the shale

gas engine is running under calibration conditions. It can be seen from the figure that when shale gas contains CO_2, the distribution area of the mapping points increases, and the number of scattered points in the upper left corner increases significantly, and the arc-shaped distribution law is obvious, showing strong non-periodic chaotic characteristics. Compared with the same content of N_2, it can be seen that the densely distributed area of the mapping points moves to the lower part of the graph, indicating that CO_2 has a stronger inhibitory effect on the combustion rate than N_2, and the cylinder pressure and pressure rise rate drop significantly; when shale gas contains 20% CO_2, the distribution range of scattered points is about 1.3～3.2MPa and 0.03～0.10MPa/°CA^{-1}, the non-periodical combustion cycle is further enhanced, and the working stability is weakened.

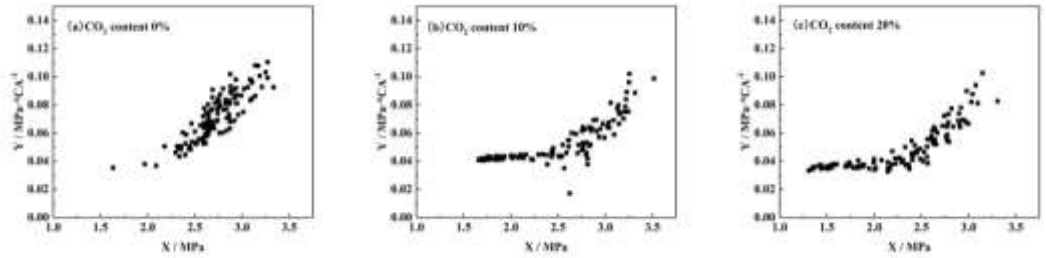

Fig. 13. Poincaré mapping of the phase space on the section $\sum XY_+$ when the CO_2 content changes

4.3. return mapping

The average indicated pressure comprehensively characterizes the pressure fluctuations of the entire cycle, and is closely related to the output power of the engine, and is an important indicator for studying engine cycle fluctuations [41-43]. **Fig. 14** shows the return map of the average indicated pressure when the engine is running at maximum torque and the content of CH_4 changes.

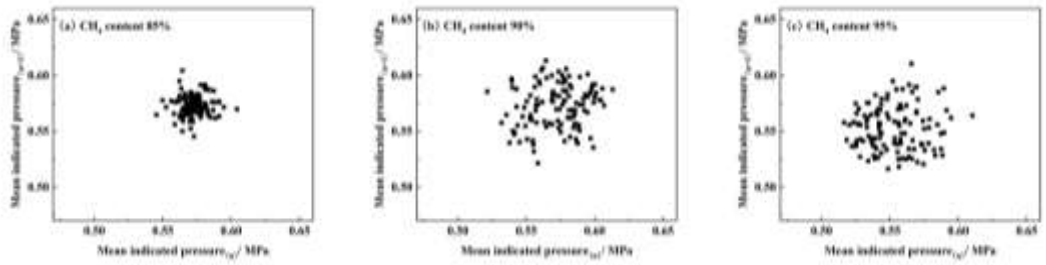

Fig. 14. The return map of the average indicated pressure time series under the maximum torque condition

It can be seen from the figure that when the CH_4 content is 85%, the return mapping points are distributed in a circular area within the range of 0.55 to 0.58 MPa, which indicates that the average indicated pressure is strongly connected during the operation of the engine, and the combustion cycle changes are determined. The combustion process is stable; when the content increases to 90%, within the circular range of 0.53～0.61MPa, the mapping points are densely distributed, and the average indicating pressure of most cycles shows a strong connection. The working process is determined, and some mapping points are randomly distributed outside the circular area, showing the randomness of the front and back cycles in the combustion cycle change process, and the working process of the engine becomes uncertain [44]; when the CH_4 content is 95%, the area where the return mapping points are densely distributed is the circular range of 0.52 to 0.61 MPa. The scattered points outside the circular range increase, the certainty of the combustion cycle variation decreases, and the combustion stability decreases.

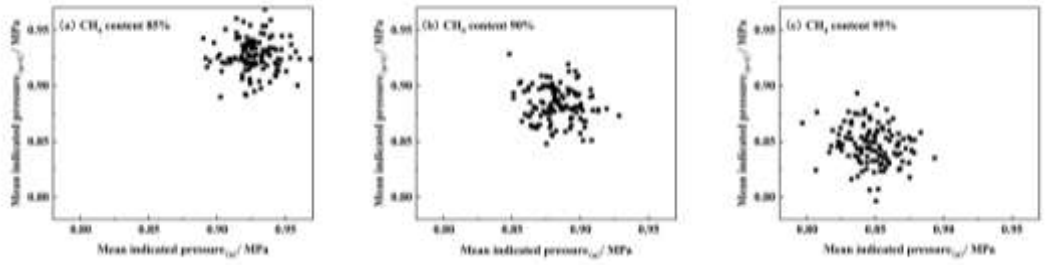

Fig. 15. The return mapping of the average indicated pressure time series of the calibration conditions

Fig. 15 shows the return map of the average indicated pressure when the engine is running under the calibrated condition and the CH_4 content changes. It can be seen from the figure that when the CH_4 content is 85%, the mapping points are mainly distributed in the upper right corner of the graphic area, the average indicating pressure is relatively large, and the distribution area is concentrated in the range of 0.90～0.96MPa. Compared with the maximum torque condition, the distribution area is increased by 0.03MPa, and the certainty of the combustion cycle change is reduced; when the CH_4 content in shale gas is 90%, the mapping point moves to the lower left corner, and the densely distributed area is 0.85～0.92MPa, some scattered points are randomly distributed outside the area, and the combustion stability decreases; when the content is 95%, the scattered points move further to the lower left corner, and the densely distributed area is about 0.81～0.89MPa; when the CH_4 content in shale gas increases, the dynamic characteristics of the combustion cycle change process gradually change from determinism to a situation where randomness and determinism coexist. The process of coexistence of randomness and determinism appears as a chaotic process.

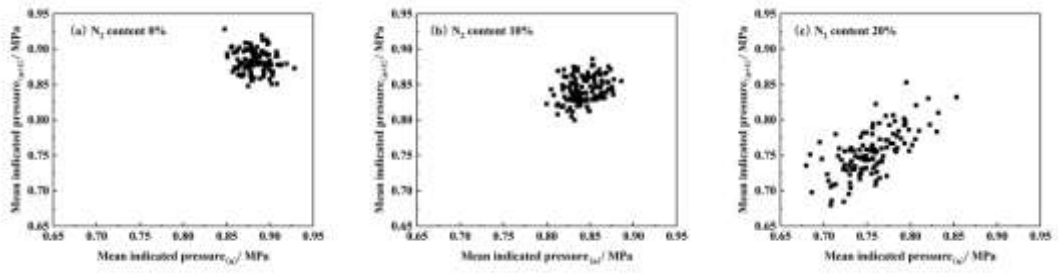

Fig. 16. The return mapping of the N_2 content change average indicating pressure time series

Fig. 16 is the return map of the average indicated pressure time series when the engine is

running under the calibrated condition and the N_2 content changes. It can be seen from the figure that when the shale gas component contains N_2, the mapping point moves to the lower left corner, the average indicated pressure decreases, the heat release rate decreases, and the combustion rate decreases. The scattered points are mainly distributed in the range of 0.80～0.88MPa. The distribution area increases, the relationship between the average indicated pressures weakens, and the combustion certainty decreases; when the N_2 content is 20%, the distribution area of the mapping points is in a belt shape, and the distribution range is significantly increased. In the lower left corner of the distribution area, there are several cycles adjacent to the average indicating low pressure, and shale gas heat is not completely released, which is a partial combustion cycle.

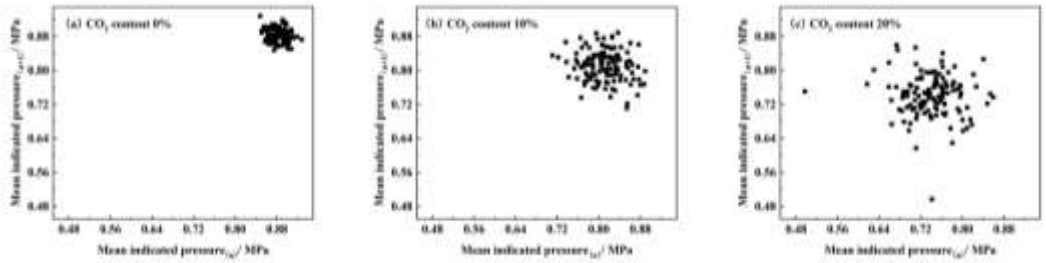

Fig. 17. Return mapping of CO_2 content change average indicating pressure time series

Fig. 17 shows the return map of the average indicated pressure time series when the engine is running under the calibration condition and the CO_2 content changes. It can be seen from the figure that when the shale gas component contains CO_2, the distribution area of the scattered points is mainly concentrated in the range of 0.72～0.89MPa. Compared with the N_2 content of 10%, the average indicated pressure decreases and the combustion rate decreases, resulting in a significant increase in the distribution range of scattered points, increasing to 0.09MPa, reducing the certainty of combustion, increasing cycle fluctuations, and increasing partial

combustion cycles; When the CO_2 content is 20%, the distribution range of the mapping points is further increased, and the area with relatively dense scatter points is concentrated in the range of 0.66～0.88MPa. Outside the dense area, the number of irregular scattered points increases, and the certainty of combustion further decreases. Part of the combustion cycle increases, there are several cycles distributed on the left side of the dense area, and the adjacent average indicating pressure is obviously smaller than the value of the dense area, indicating that the combustion is not proceeding, and it is a misfire cycle.

4.4. Chaotic characteristics of the combustion process

(1) Association dimension

Fig. 18 shows the correlation dimension of the reconstructed phase space trajectory when the shale gas engine is operated under the maximum torque condition and the calibration condition, and the CH_4 content changes. It can be seen from the figure that the engine is operating under the maximum torque condition and when the CH_4 content in shale gas is 85%, the correlation dimension of the phase space trajectory is 1.65. When the CH_4 content increases, the correlation dimension increases, indicating that the complexity of the combustion system attractor increases, and the combustion rate decreases, which leads to an increase in heat release time, an increase in cycle variation coefficient, and a decrease in combustion stability. When the content is 95%, the correlation dimension increases to 1.69; when the shale gas engine is operating under the calibration conditions, the correlation dimension of the phase space trajectory increases significantly. When the CH_4 content is 85%, the correlation dimension is 1.73, an increase of 0.08, It shows that the complexity of the attractor is obviously increased,

the distribution range of the phase space trajectory is increased, the unpredictability of the overall working state of the engine is increased, and the combustion stability is decreased. The main reason is that the engine speed increases, the charging efficiency in the cylinder decreases, and the flame propagation is difficult; similar to the maximum torque condition, during the calibration condition, with the increase of the CH_4 content in the shale gas, the correlation dimension increases linearly. When the volume fraction is 95%, the correlation dimension reaches 1.79.

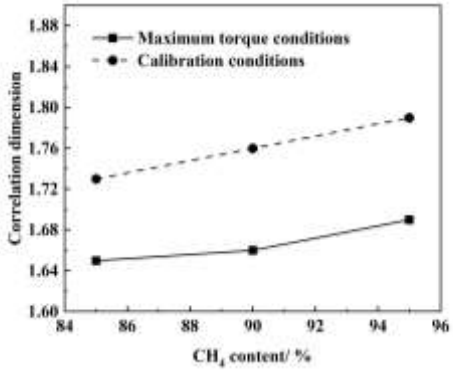

Fig. 18. Correlation dimension under different CH_4 content

Fig. 19 shows the correlation dimension of reconstructed phase space trajectory with different contents of N_2 and CO_2 in shale gas when the engine is running under calibration conditions. It can be seen from the figure that when the shale gas component does not contain inert gas, the correlation dimension of the phase space trajectory is 1.76. When the N_2 content is 10%, the flame propagation speed of shale gas decreases and the combustion stability decreases. The complexity of the phase space trajectory attractor increases, the distribution range of the trajectory increases, the correlation dimension increases to 1.80, and when the N_2 content increases to 20%, the correlation dimension further increases, and the increase is increased by 0.01 to 1.85. The distribution range of the phase space trajectory increases, and

508 the combustion stability decreases; when the shale gas contains 10% CO_2, the correlation
509 dimension of the phase space trajectory increases to 1.81, which is higher than when the N_2
510 content is 10%. It is greater than 0.01, indicating that CO_2 has a stronger inhibitory effect on
511 combustion than N_2, the combustion rate decreases more, the complexity of the phase space
512 trajectory is increased, and the unpredictability of the combustion process is enhanced. When
513 the CO_2 content is 20%, the correlation dimension increases significantly, reaching 1.88,
514 indicating that when the shale gas contains 20% CO_2, the difficulty of flame propagation has
515 increased significantly, the burning rate has decreased significantly, the unpredictability of the
516 phase space trajectory has increased, and the combustion stability has decreased significantly
517 [45-46].

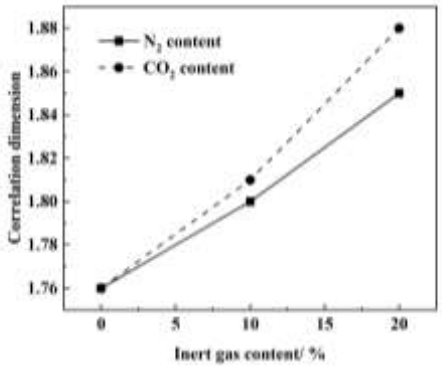

518

519 **Fig. 19.** Correlation dimension under different contents of inert gas

520 (2) The largest Lyapunov exponent

521 **Fig. 20** shows the maximum Lyapunov exponent of the time series of the in-cylinder pressure
522 when the shale gas engine is operating under the maximum torque and calibration conditions,
523 and the CH_4 content changes.

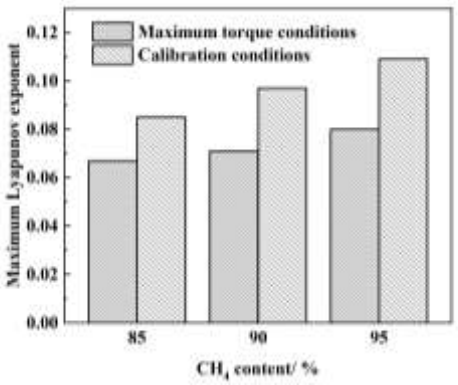

Fig. 20. The largest Lyapunov exponent under different CH_4 content

It can be seen from the figure that when the engine is operating at the maximum torque, the maximum Lyapunov index is 0.067 when the CH_4 content is 85%. With the increase of CH_4 content, the index increases, indicating that when the CH_4 content in shale gas increases, the periodicity of the cylinder pressure time series decreases, the degree of chaos increases, the volume fraction increases to 95%, and the index increases by 0.013 to 0.080; when the shale gas engine is running under the calibration condition, when the CH_4 content is 85%, the maximum Lyapunov exponent reaches 0.085, which is 0.018 more than the maximum torque condition, and the combustion stability of the engine decreases; In the calibration condition, with the increase of CH_4 content, the maximum Lyapunov exponent increases. When the CH_4 content is 90% and 95%, the index increases by 0.012 respectively. Compared with the maximum torque operating condition, the exponential increase rate increases, indicating that when the shale gas engine speed increases, the time series of the in-cylinder pressure is more sensitive to the increase of CH_4 content, the cycle changes are large, and the combustion stability is poor.

Fig. 21 shows the maximum Lyapunov exponent of the cylinder pressure time series with different contents of N_2 and CO_2 in shale gas when the engine is running under the calibrated

conditions. It can be seen from the figure that when the shale gas does not contain inert gas, the maximum Lyapunov exponent is 0.097. As the N_2 content increases, the index gradually increases, the chaotic degree of the cylinder pressure time series increases, the periodicity decreases, and the combustion is stable. When the content is 20%, the index reaches 0.129, an increase of 32.9%; when the CO_2 content in shale gas is 10%, the maximum Lyapunov index is 0.115, which is an increase of 0.004 compared to when the N_2 content is 10%. It shows that under the same volume fraction, the in-cylinder pressure time series is more sensitive to CO_2 content, and the combustion is more unstable. When the content is 20%, the maximum Lyapunov exponent is 0.138, the increase is the largest, and the cycle change increases significantly.

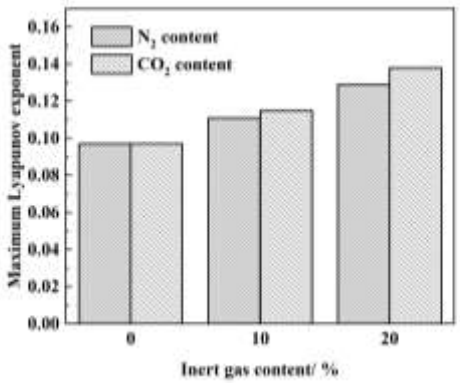

Fig. 21. The maximum Lyapunov exponent under different contents of inert gas

5. Conclusion

Using methods such as phase space reconstruction, Poincaré mapping, and return mapping, researches have been carried out on the nonlinear dynamic characteristics of shale gas engine combustion cycle changes. The research shows that:

(1) During the working process of a shale gas engine, the pressure in the cylinder shows a

quasi-periodical state in the entire phase space, and the working process has a certain chaotic law; the phase space trajectory has a higher degree of coincidence during the intake and exhaust phases, the pressure in the cylinder fluctuates greatly in the combustion phase, the trajectory is arc-shaped, and the arrangement is more dispersed; As the content of CH_4, N_2 and CO_2 in shale gas increases, the combustion cycle changes increase, the trajectory of the arc segment is gradually dispersed, and the randomness of the engine working process increases.

(2) The phase space trajectory has a monotonically increasing distribution of the Poincaré mapping points on the $\sum XY_+$ section. When the shale gas engine has a small cycle change, the scattered points are distributed in an elliptical shape, and the distribution range is small, and the engine working process has a strong periodicity, with the increase of the combustion cycle, the linear relationship of the scattered points gradually increases. At the lower left corner of the distribution area, some of the scattered points rise upward, and the randomness of the combustion process increases.

(3) The return mapping points of the engine combustion characteristic parameters are distributed in a cluster. When the CH_4 content in shale gas increases, the distribution range of the average indicated pressure return mapping points increases, indicating that the randomness of the engine working process increases and the stability of the combustion process decreases; with the increase of N_2 and CO_2 content, on the left and lower sides of the scatter-intensive area, several cycles of mapping points are randomly distributed, indicating that abnormal combustion such as partial combustion or misfire occurs during engine combustion. The uncertainty of the process increases.

(4) With the increase of engine speed, the correlation dimension and the maximum Lyapunov

exponent increase, the randomness of the combustion process increases, and the chaotic characteristics of the engine working process are obvious; the time series of the cylinder pressure is more sensitive to the content of inert gas. With the increase of N_2 and CO_2 content in the gas, the correlation dimension and the maximum Lyapunov exponent increase significantly, the complexity of the phase space trajectory increases, and the chaotic characteristics become more obvious.

Declaration of Competing Interest

The authors declare that they have no known competing financial interests or personal relationships that could have appeared to influence the work reported in this paper.

Acknowledgements

This study was supported by the National Natural Science Foundation of China under Grant (No. 51776089), Natural science research projects in Jiangsu higher education institutions (18KJB470006), Zhenjiang Key R&D Program-Social Development (SH2020006), the Open Research Subject of Key Laboratory of Automobile Measurement and Control and Safety (QCCK2019-004).

References

[1] Ran Z, Hariharan D, Lawler B, et al. Experimental study of lean spark ignition combustion using gasoline, ethanol, natural gas, and syngas[J]. Fuel, 2019, 235(JAN.1):530-537.

601 [2] Zuohua, Huang, Bing, et al. Experimental Study on Engine Performance and Emissions for an Engine
602 Fueled with Natural Gas−Hydrogen Mixtures[J]. Energy & Fuels, 2006.
603 [3] A L P Y, A E Z S, A S L D, et al. Analysis of the dynamic characteristics of combustion instabilities
604 in a pre-mixed lean-burn natural gas engine - ScienceDirect[J]. Applied Energy, 2016, 183:746-759.
605 [4] Poorghasemi K, Saray R K, Ansari E, et al. Effect of diesel injection strategies on natural gas/diesel
606 RCCI combustion characteristics in a light duty diesel engine[J]. Applied Energy, 2017,
607 199(AUG.1):430-446.
608 [5] Clarkson C R, Freeman M, He L, et al. Characterization of tight gas reservoir pore structure using
609 USANS/SANS and gas adsorption analysis[J]. Fuel, 2012, 95:371-385.
610 [6] Bo G. Geochemical Characteristics of Shale Gas from Lower Silurian Longmaxi Formation in the
611 Sichuan Basin and Its Geological Significance[J]. Natural Gas Geoence, 2016, 1(2):119-129.
612 [7] Ladd J W, Olsen D B, Beshouri G. Evaluation of operating parameters and fuel composition on knock
613 in large bore two-stroke pipeline engines[J]. Fuel, 2017, 202(aUG.15):165-174.
614 [8] Tayari F, Blumsack S. A real options approach to production and injection timing under uncertainty
615 for CO2 sequestration in depleted shale gas reservoirs[J]. Applied Energy, 2020, 263.
616 [9] Kumar M R, Hao D, Sijie L, et al. Experimental and artificial neural network (ANN) study of
617 hydrogen enriched compressed natural gas (HCNG) engine under various ignition timings and
618 excess air ratios[J]. Applied Energy, 2018, 228:736-754.
619 [10] Zhenzhong Yang, Zhang F, Wang L, et al. Effects of injection mode on the mixture formation and
620 combustion performance of the hydrogen internal combustion engine[J]. Energy, 2018.
621 [11] Gascoin N, Yang Q, Chetehouna K. Thermal Effects of CO2 on the NOx Formation Behavior in the
622 CH4 Diffusion Combustion System[J]. Applied Thermal Engineering, 2017, 110:144-149.

623 [12] Pischinger S, Marco Günther, Budak O. Abnormal combustion phenomena with different fuels in a
624 spark ignition engine with direct fuel injection[J]. Combustion and Flame, 2017.
625 [13] Cheng Q, Ahmad Z, Kaario O, et al. Cycle-to-cycle variations of dual-fuel combustion in an
626 optically accessible engine[J]. Applied Energy, 2019, 254.
627 [14] Li W, Liu Z, Wang Z, et al. Experimental and theoretical analysis of effects of N2, O2 and Ar in
628 excess air on combustion and NOx emissions of a turbocharged NG engine[J]. Energy Conversion
629 and Management, 2015.
630 [15] Corey E. Weaver, Domenic A. Santavicca. Correlation of Cycle-Resolved Flame Kernel Growth
631 and Cylinder Pressure Measurements in An Optically-Accessible Engine, SAE Paper, 922171, 1992
632 [16] Li Congxin, Zhang Xin, Hu Zhunqing, et al. Experimental Study on Combustion and Emission
633 Performance of Engine Fueled with Coal Bed Gas[J]. Internal Combustion Engine Engineering,
634 2009, 30(5):31-35
635 [17] Daw C S, Green J B, Kennel M B, et al. A simple model for cyclic variations in a spark-ignition
636 engine[J]. Office of Scientific & Technical Information Technical Reports, 2001.
637 [18] J.B. Green, Jr., C.S. Daw, J.S. Armfield, C.E.A. Finney, R.M. Wagner, J.A. Drallmeier, M.B.Kennel,
638 P Durbetaki, Time irreversibility and comparison of cyclic variability models, SAE Paper, No. 1999-
639 01-0221, 1999.
640 [19] R.M.Wangner, J.A.Drallmeier, C.S.Daw, Prior-cycle effects in lean spark ignition combustion-
641 fuel/air charge considerations, SAE Paper, No.981047, 1998.
642 [20] Yao Baofeng, Li Guoxiu. Analysis and Research on Characteristic Parameters of Natural Gas Engine
643 Combustion Cycle[J]. Internal Combustion Engine Engineering, 2007, 28(4):1-5.
644 [21] Yang L P, Bodisco T A, Zare A, et al. Analysis of the nonlinear dynamics of inter-cycle combustion

645 variations in an ethanol fumigation-diesel dual-fuel engine[J]. Nonlinear Dynamics, 2019,
646 95(3):2555-2574.
647 [22] C. Letellier, S. Meunier-Guttin-Cluzel, G Gouesbet, F. Neveu, T. Duverger, B. Cousyn, Use of the
648 nonlinear dynamical system theory to study cycle-by-cycle variations from spark ignition engine
649 pressure data, SAE Paper, No. 97164, 1997.
650 [23] Liu Shuai Wang Zhong Zhao Yang Qu Lei Sun Bo. Nonlinear dynamics analysis for combustion
651 stability of spark-ignition engine. 2016, 32(14):69-75.
652 [24] Wang Liyuan, Yang Liping, Ma Xiuzhen,Li Jun. Analysis of Chaotic Combustion Process of Spark
653 Ignition Natural Gas Engine[J]. Journal of Beijing University of Technology,2012,38(05):689-694.
654 [25] Ding S L, Song E Z, Yang L P, et al. Analysis of chaos in the combustion process of premixed natural
655 gas engine[J]. Applied Thermal Engineering, 2017.
656 [26] Yao B, Yan H U, Guanqin M A, et al. In-Cylinder Pressure Data Acquisition and Analysis of Cycle-
657 to-Cycle Variations in A Nature Gas Engine[J]. Journal of Beijing Jiaotong University, 2008.
658 [27] Ding S L, Song E Z, Yang L P, et al. Effects of injection timing on nonlinear dynamics of the
659 combustion process in the lean-burn premixed natural gas engine[J]. The European Physical Journal
660 Plus, 2017, 132(2):90.
661 [28] Martynova I. On evaluation of the topological degree of the Poincare map in some singular
662 situations[J]. Science, 2010, 3(1):40-44.
663 [29] Shamolin M V. Classes of Variable Dissipation Systems with Nonzero Mean in the Dynamics of a
664 Rigid Body[J]. Journal of Mathematical Sciences, 2004, 122(1):2841-2915.
665 [30] Shujun Li, Guanrong Chen, Gonzalo álvarez. Return-map Cryptanalysis Revisited. 2006,
666 16(5):1557-1568.

667 [31] Czarnigowski J. A simple method of analysis and modelling of cycle-to-cycle variation of engine
668 work-the example of indicated pressure[J]. SAE International. Lublin, Poland: Engine Combustion,
669 Thermal Engineering Computer Application, 2007: 655－661.
670 [32] Nowak M A, May R M. Evolutionary Games and Spatial Chaos. [J]. Nature, 1992, 359(6398):826-
671 829.
672 [33] Stephens N G, Parsons A, Brown M J, et al. Randomised controlled trial of vitamin E in patients
673 with coronary disease: Cambridge Heart Antioxidant Study (CHAOS)[J]. Lancet, 1996,
674 347(9004):311–316.
675 [34] Malhotra R, Holman M, Ito T. Chaos and stability of the solar system. [J]. Proceedings of the
676 National Academy of Sciences of the United States of America, 2001, 98(22):12342-3.
677 [35] Procaccia I, Grassberger P, Hentschel H G E. On the characterization of chaotic motions[M]//
678 Dynamical System and Chaos. Springer Berlin Heidelberg, 1983.
679 [36] Sun Y, Rao Z, Zhao D, et al. Characterizing nonlinear dynamic features of self-sustained
680 thermoacoustic oscillations in a premixed swirling combustor[J]. Applied Energy, 2020, 264.
681 [37] Sen A K, Litak G, Kaminski T, et al. Multifractal and statistical analyses of heat release fluctuations
682 in a spark ignition engine. [J]. Chaos (Woodbury, N.Y.), 2008, 18(3):033115.
683 [38] Davis M J, Tomlin AS. Spatial dynamics of steady flames 1. Phase space structure and the dynamics
684 of individual trajectories. [J]. Journal of Physical Chemistry A, 2008, 112(34):7768-7783.
685 [39] Maldonado, Bryan, P, et al. Cycle-to-Cycle Feedback for Combustion Control of Spark Advance at
686 the Misfire Limit[J]. Journal of Engineering for Gas Turbines & Power Transactions of the Asme,
687 2018.
688 [40] Singaravelu B, Mariappan S. Stability analysis of thermoacoustic interactions in vortex shedding

689 combustors using Poincaré map[J]. Journal of Fluid Mechanics, 2016, 801:597-622.

690 [41] Hunicz J, Mikulski M, Geca M S, et al. An applicable approach to mitigate pressure rise rate in an

691 HCCI engine with negative valve overlap[J]. Applied Energy, 2020, 257.

692 [42] Wang L Y, Yang L P, Song E Z, et al. Effect of Port Gas Injection on the Combustion Instabilities in

693 a Spark-Ignition Lean-Burn Natural Gas Engine[J]. International Journal of Bifurcation and Chaos,

694 2018, 28(10):1850124.

695 [43] Momir Sjerić, Ivan Taritaš, Rudolf Tomić, et al. Efficiency improvement of a spark-ignition engine

696 at full load conditions using exhaust gas recirculation and variable geometry turbocharger –

697 Numerical study[J]. Energy Conversion and Management, 2016, 125:26-39.

698 [44] Yu Shui, Dong Guangyu, Gao Gao, et al. Transient combustion characteristics of engines at fast start

699 based on cycle analysis[J]. Journal of Internal Combustion Engine, 2008, 26(5):404-409.

700 [45] Keskinen J P, Vuorinen V, Kaario O. Nonlinear time series analysis from large eddy simulation of

701 an internal combustion engine[J]. International Journal of Heat & Fluid Flow, 2016, 57(feb.):79-90.

702 [46] Kaewpradap A, Jugjai S. Experimental study of flame stability enhancement on lean premixed

703 combustion of a synthetic natural gas in Thailand[J]. Energy, 2019, 188:116029-.

Figures

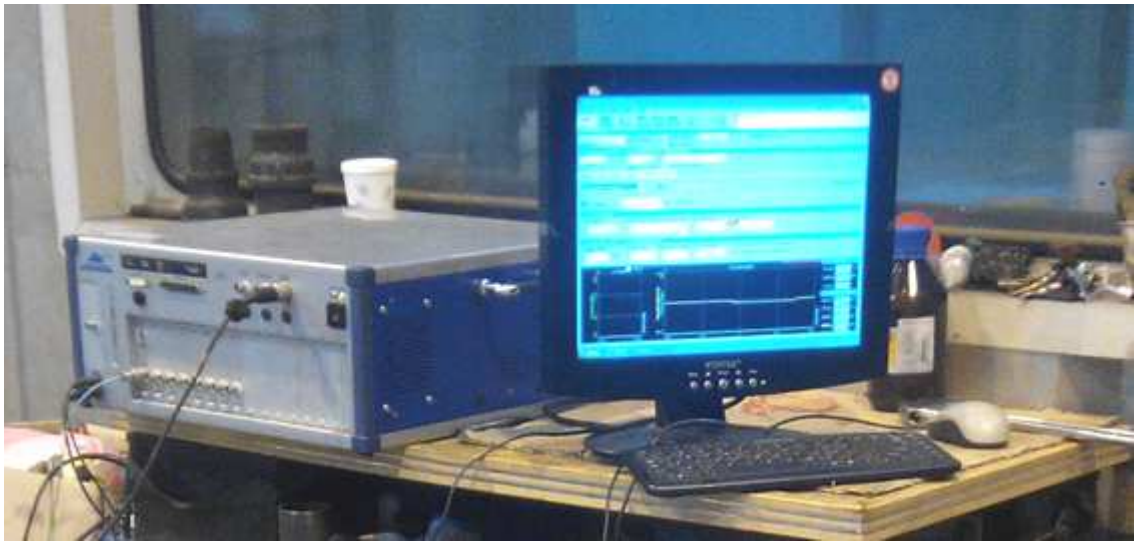

Figure 1

DEWE800 combustion analyzer

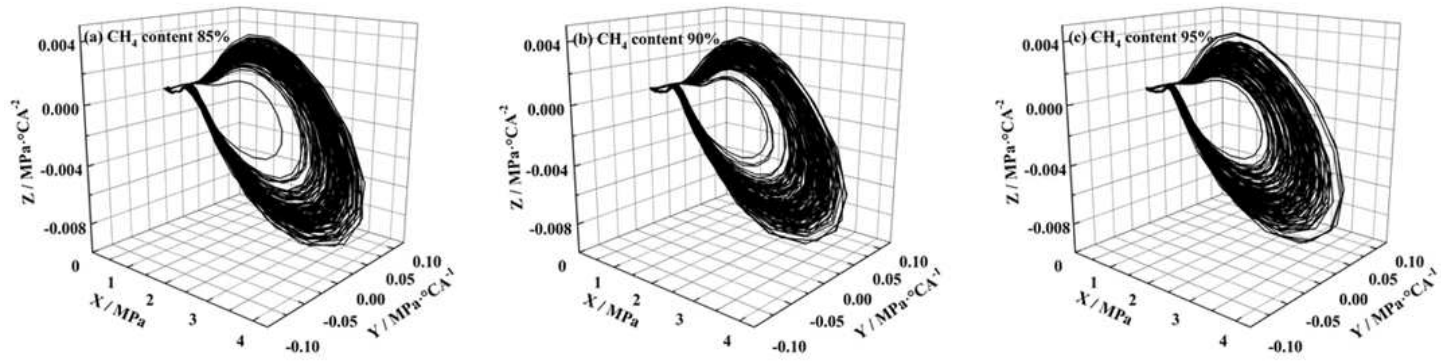

Figure 2

The phase space of the combustion process in the cylinder under the maximum torque condition

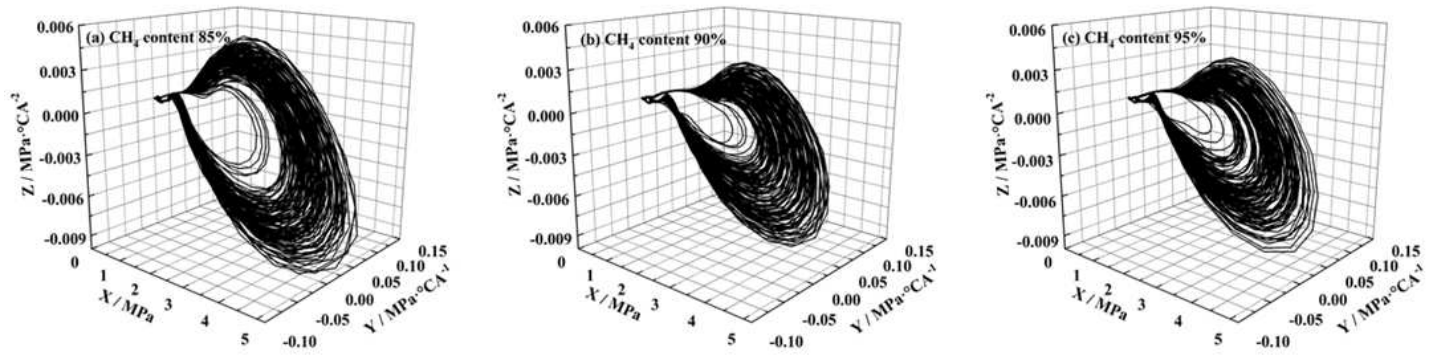

Figure 3

The phase space of the combustion process in the cylinder under calibration conditions

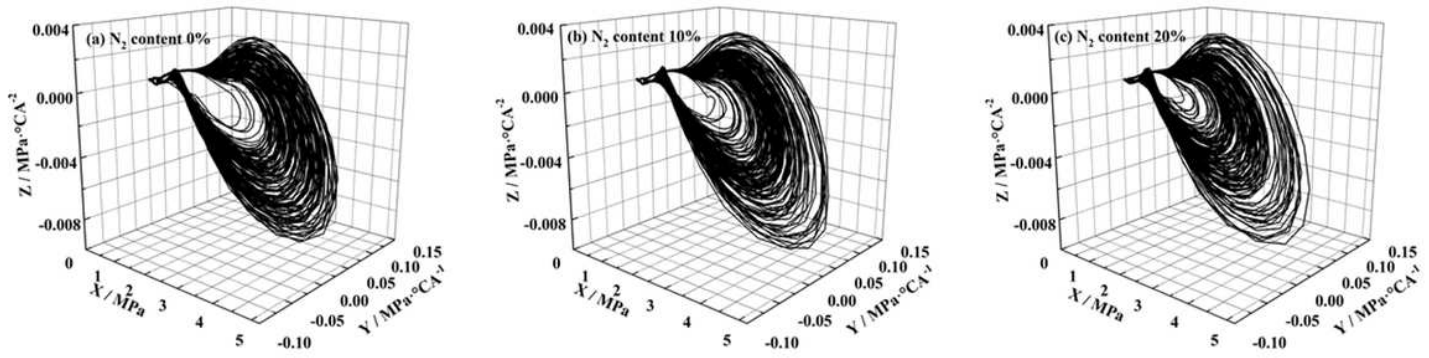

Figure 4

The phase space of the combustion process in the cylinder when the N2 content changes

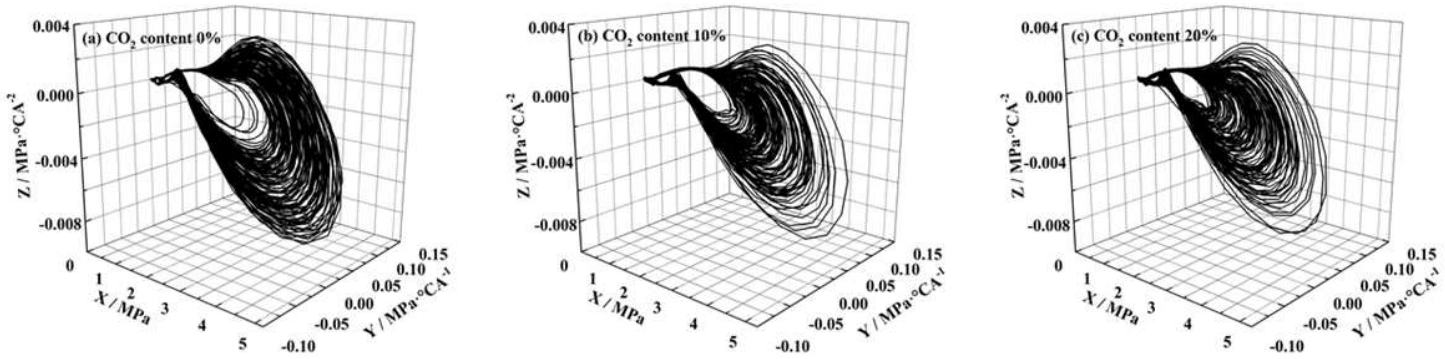

Figure 5

The phase space of the combustion process in the cylinder when the CO2 content changes

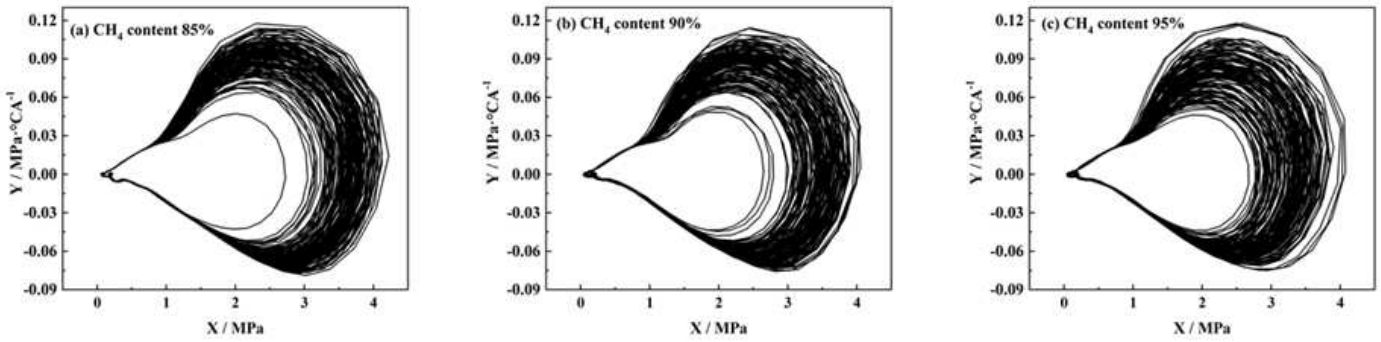

Figure 6

Projection of phase space trajectory on XY plane for maximum torque condition

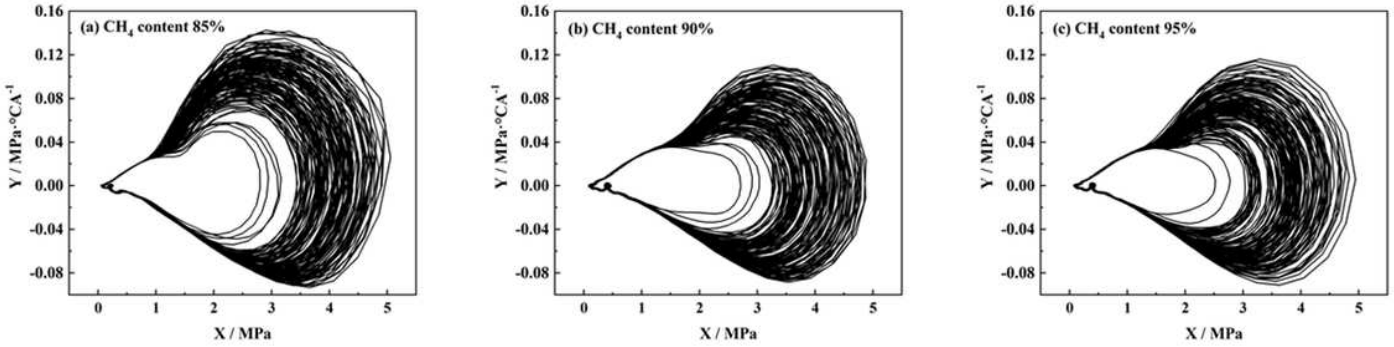

Figure 7

The projection of the phase space trajectory on the XY plane of the calibration condition

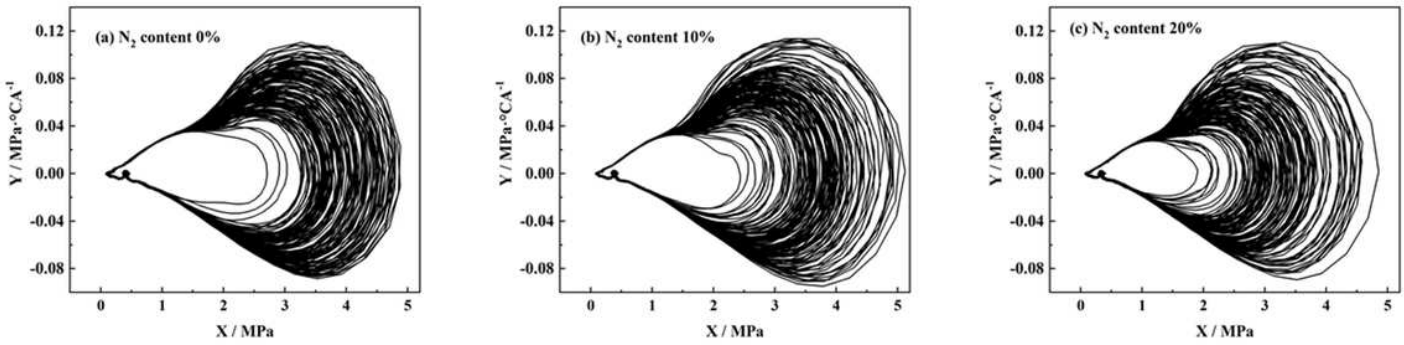

Figure 8

Projection of phase space trajectory on XY plane when N2 content changes

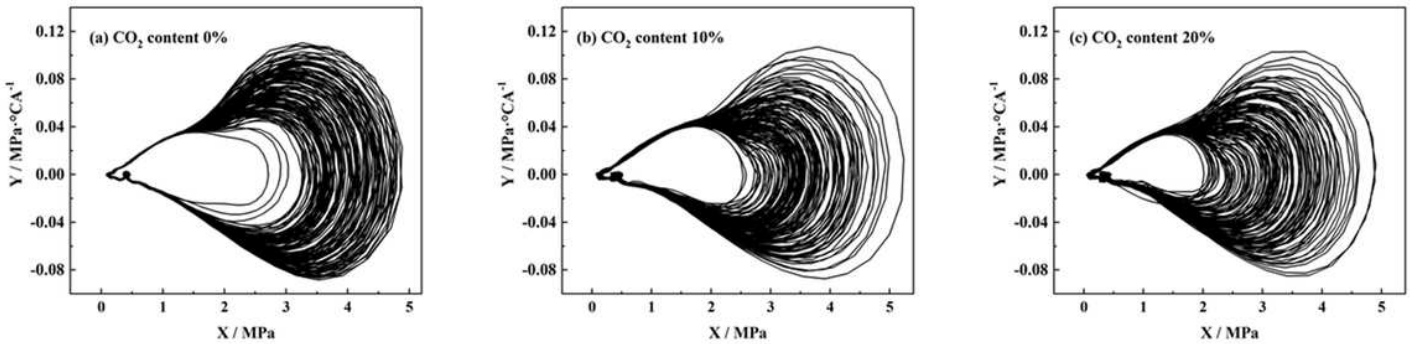

Figure 9

Projection of phase space trajectory on XY plane when CO2 content changes

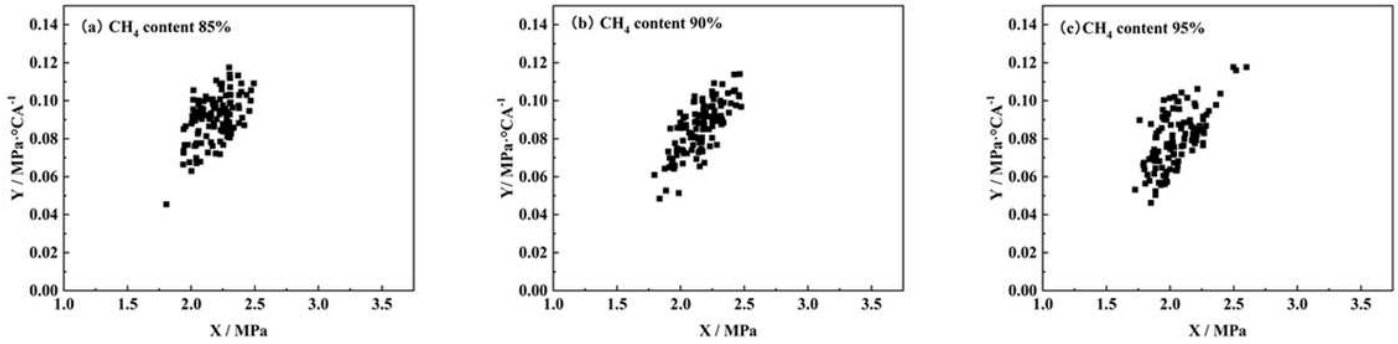

Figure 10

Poincaré mapping of the phase space of the maximum torque condition on the section ∑XY+

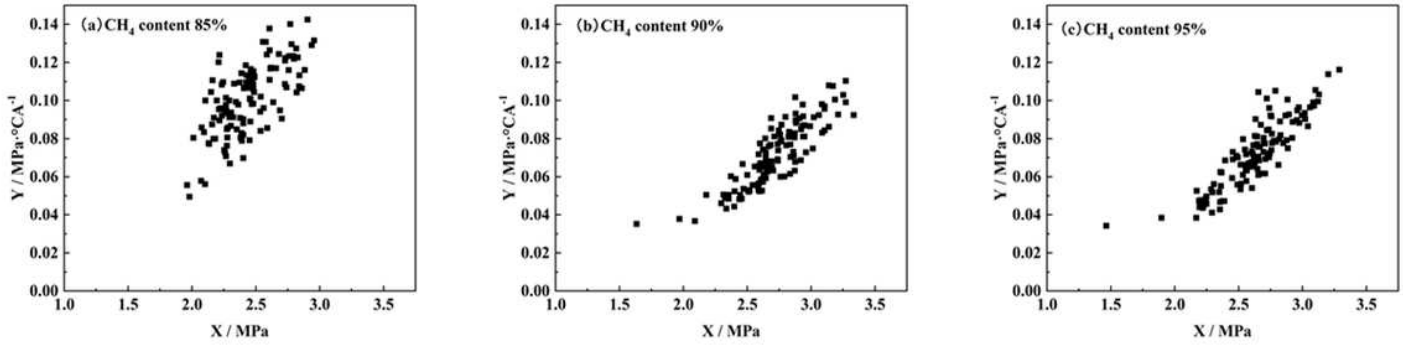

Figure 11

The Poincaré mapping of the phase space of the calibrated condition on the section ∑XY+

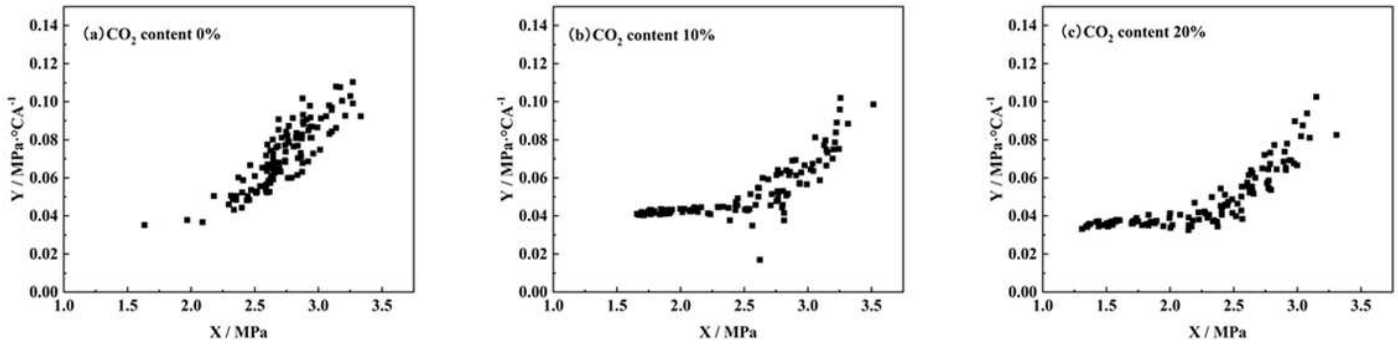

Figure 13

Poincaré mapping of the phase space on the section ∑XY+ when the CO2 content changes

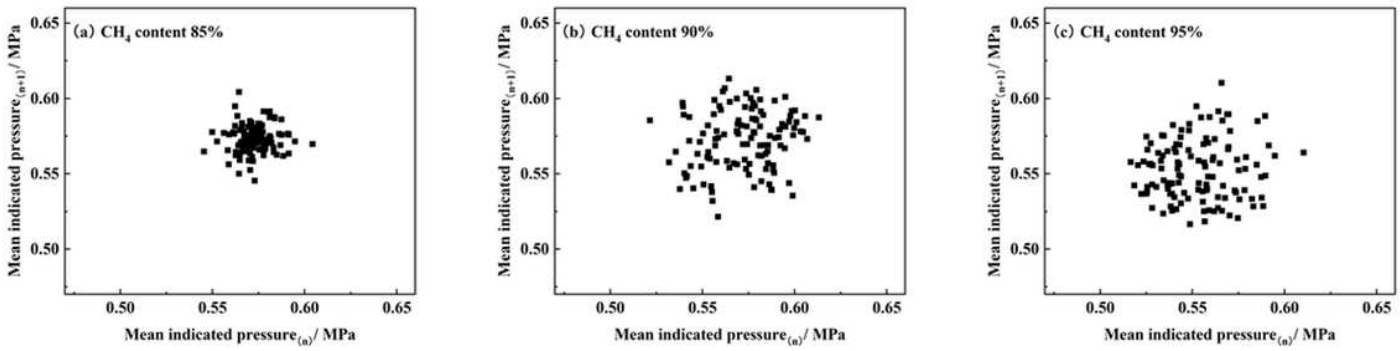

Figure 14

The return map of the average indicated pressure time series under the maximum torque condition

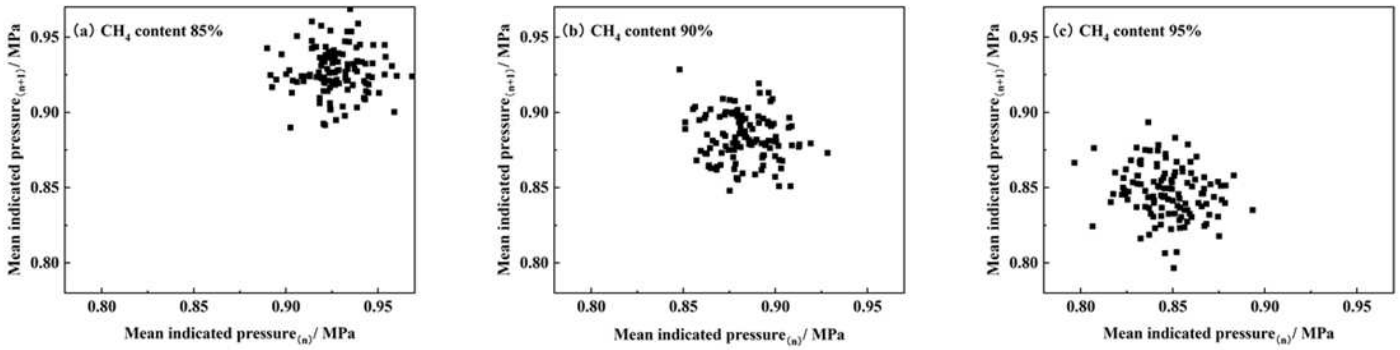

Figure 15

The return mapping of the average indicated pressure time series of the calibration conditions

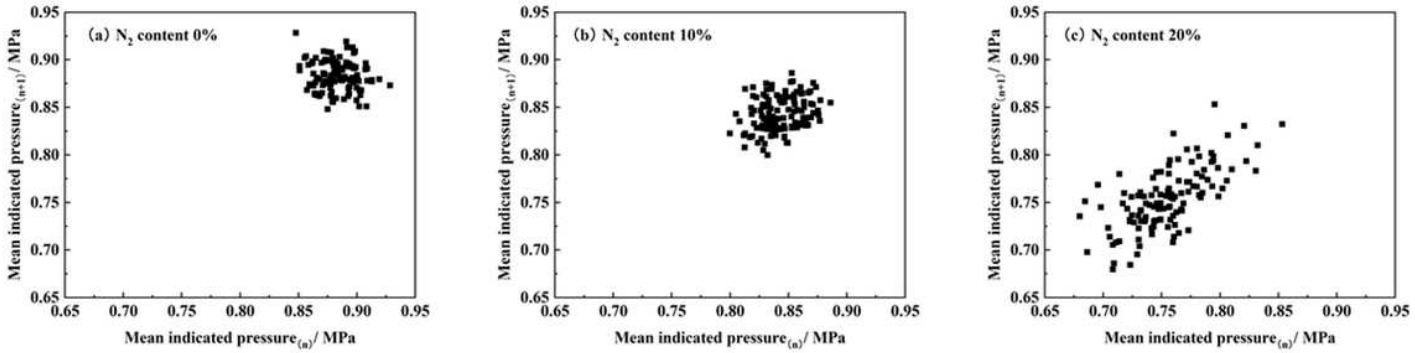

Figure 16

The return mapping of the N2 content change average indicating pressure time series

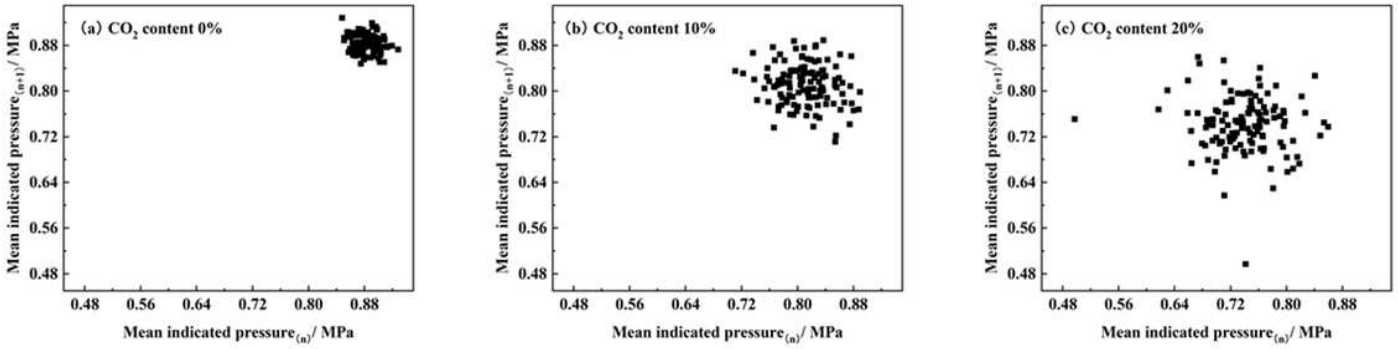

Figure 17

Return mapping of CO2 content change average indicating pressure time series

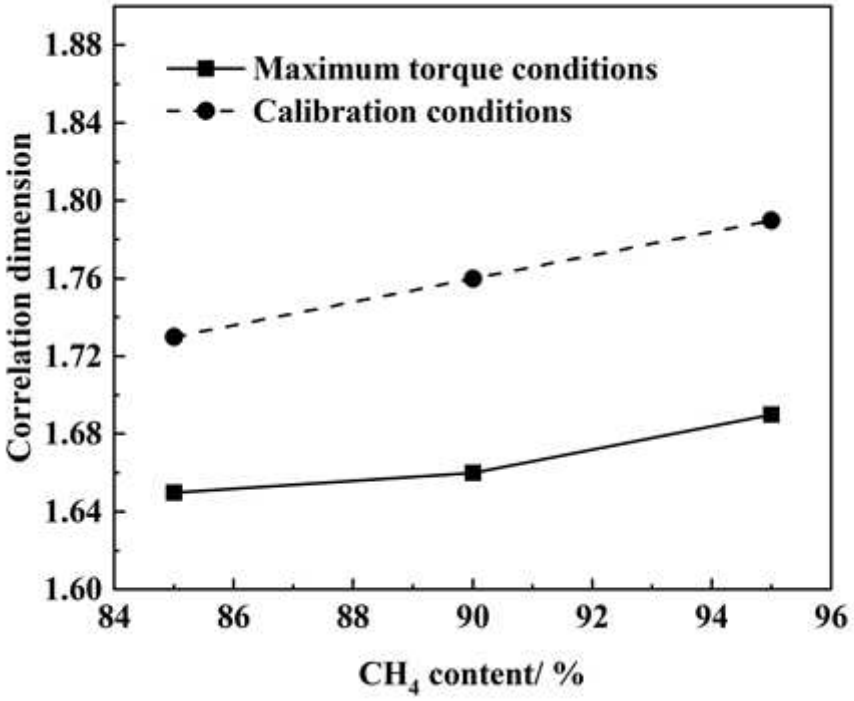

Figure 18

Correlation dimension under different CH4 content

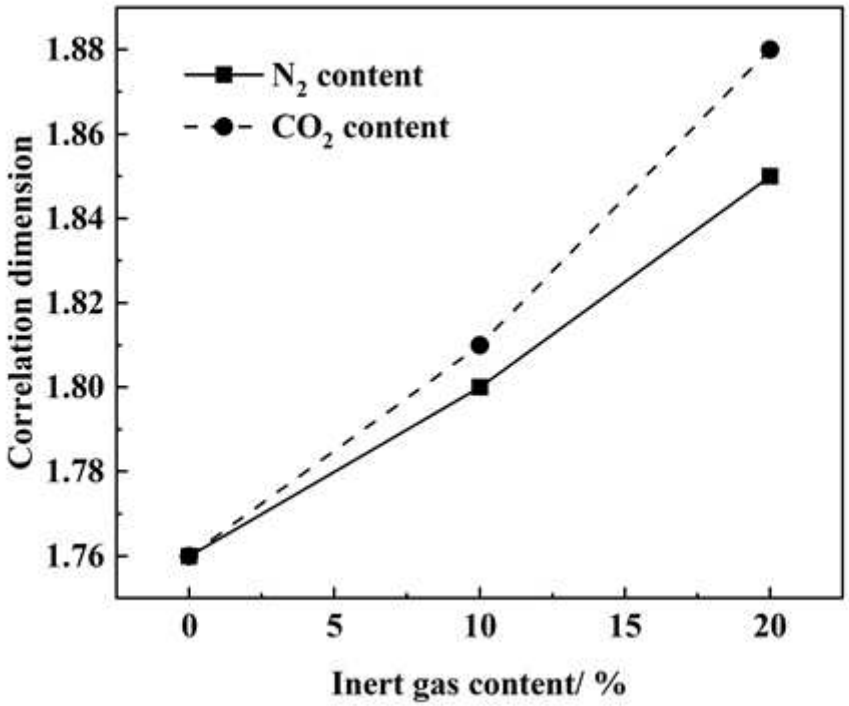

Figure 19

Correlation dimension under different contents of inert gas

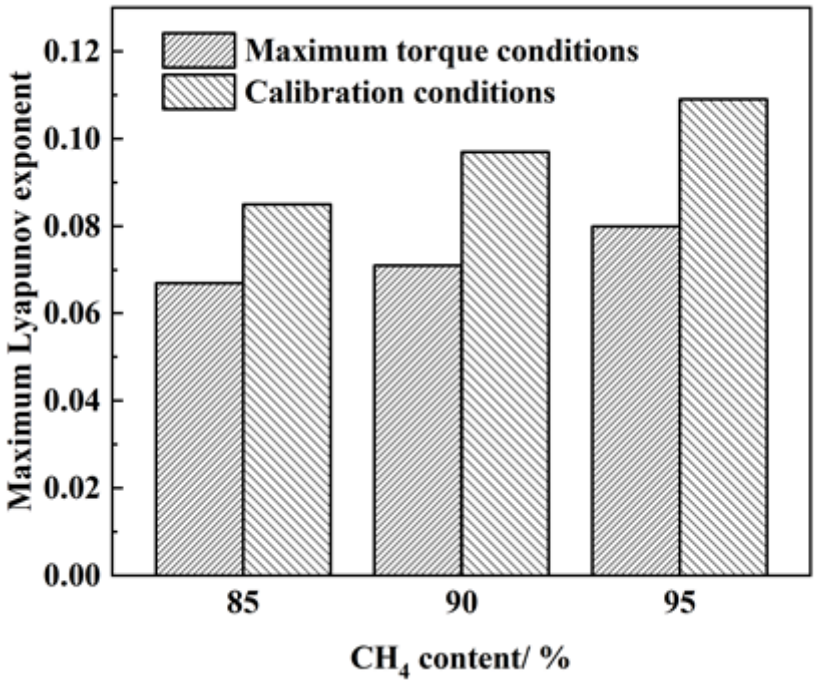

Figure 20

The largest Lyapunov exponent under different CH4 content

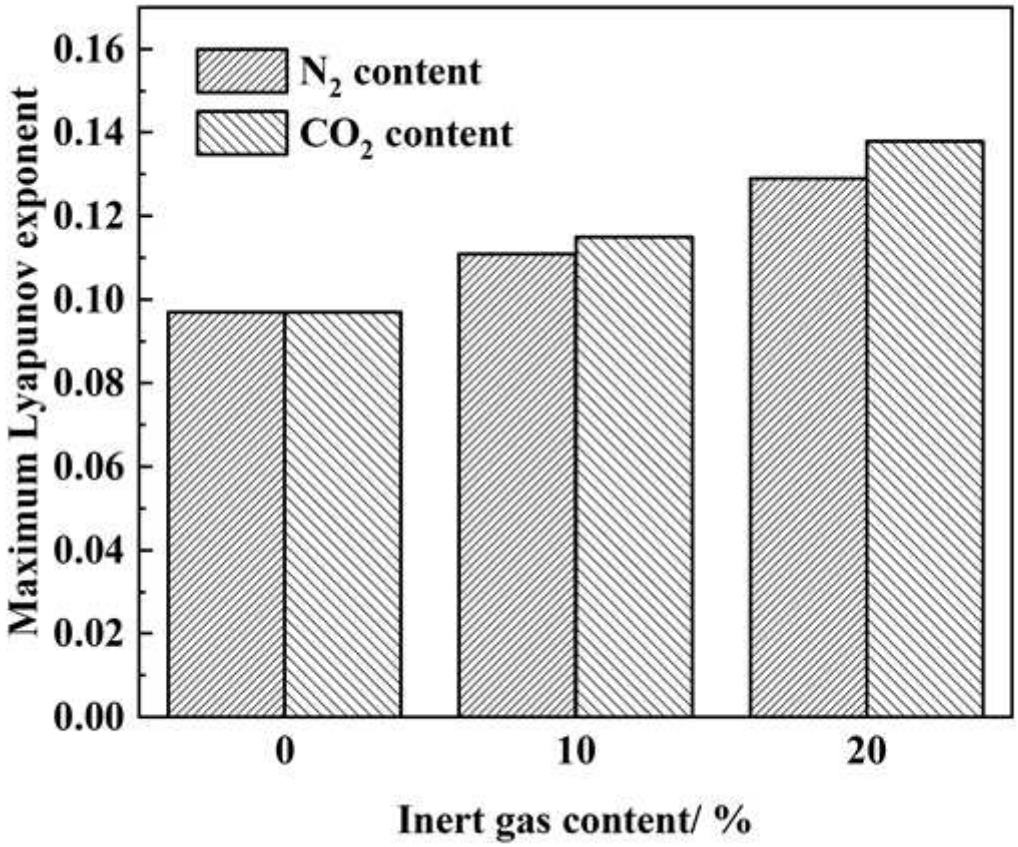

Figure 21

The maximum Lyapunov exponent under different contents of inert gas